Dynamic modulation yields one-way beam splitting

Sajjad Taravati[1,2,*] and Ahmed A. Kishk[1]

[1]*Department of Electrical and Computer Engineering, Concordia University, Montréal, Quebec, Canada H3G 2W1*

[2]*Department of Electrical and Computer Engineering, University of Toronto, Toronto, Ontario, Canada M5S 2E4*

(Received 22 June 2018; revised manuscript received 6 January 2019; published 1 February 2019)

This paper demonstrates the realization of an extraordinary beam splitter, exhibiting one-way beam splitting amplification. Such a dynamic beam splitter operates based on nonreciprocal and synchronized photonic transitions in obliquely illuminated space-time-modulated (STM) slabs which impart the coherent temporal frequency and spatial frequency shifts. As a consequence of such unusual photonic transitions, a one-way beam splitting is exhibited by the STM slab. Beam splitting is a vital operation for various communication systems, including circuit quantum electrodynamics, and signal-multiplexing and demultiplexing. Despite that the beam splitting is conceptually a simple operation, the performance characteristics of beam splitters significantly influence the repeatability and accuracy of the entire system. As of today, there has been no approach exhibiting a nonreciprocal beam splitting accompanied with transmission gain and an arbitrary splitting angle. Here, we show that oblique illumination of a periodic and semicoherent dynamically-modulated slab results in coherent photonic transitions between the incident light beam and its counterpart space-time harmonic (STH). Such transitions introduce a unidirectional synchronization and momentum exchange between two STHs with same temporal frequencies but opposite spatial frequencies. Such a beam splitting technique offers high isolation, transmission gain, and zero beam tilting, and is expected to drastically decrease the resource and isolation requirements in communication systems. In addition to the analytical solution, we provide a closed-form solution for the electromagnetic fields in STM structures, and accordingly, investigate the properties of the wave isolation and amplification in subluminal, superluminal, and luminal ST modulations.

DOI: 10.1103/PhysRevB.99.075101

I. INTRODUCTION

Beam splitters are quintessential elements of communication systems [1–7]. In the microwave regime, beam splitters are required for the generation of single photons in the circuit quantum electrodynamics [1,8–13], heterodyne mixer arrays [3], and wave engineering and signal-multiplexing and demultiplexing [4–7]. However, the realization of microwave on-chip beam splitters is still under research and development [1,2,14]. In spite of the immense scientific attempts for the realization of efficient beam splitters, beam splitters are restricted to reciprocal response and suffer from substantial transmission loss. As a consequence, the resource requirements of the overall system, including demand for high power microwave sources and isolators, will be increased.

This paper presents the application of space-time-modulated (STM) structures to extraordinary beam splitting. As of today, various applications of STM structures have been reported, where normal incidence of the light beam to the STM structure yields unusual interaction with electromagnetic wave [15–21]. These applications include but are not limited to the parametric traveling-wave amplifiers [22–25], isolators [18,26–32], metasurfaces [33–36], pure frequency mixer [37], circulators [38–40], and mixer-duplexer-antenna system [41,42]. Nevertheless, there has been a lack of investigation on the properties of STM media under oblique incidence and its applications.

Here, we introduce a one-way, tunable, and highly efficient beam splitter and amplifier based on coherent photonic transitions through the oblique illumination of STM structures. The contributions of this paper are as follows.

(1) In contrast to conventional beam splitters which are restricted to reciprocal response with more than 3 dB insertion loss, the proposed STM beam splitter is capable of providing nonreciprocal response with transmission gain. It can also be used in antenna applications, where the transmitted and received waves are engineered appropriately.

(2) We show that the STM beam splitter presents an efficient performance for both collimated and noncollimated incidence beam with no output beam tilt. This is very interesting as conventional passive beam splitters suffer from poor performance for noncollimated beams and provide an undesired output beam tilt.

(3) It is demonstrated that the angle of transmission and the amplitude of the transmitted beams depend on the ST modulation parameters. Hence, the ST modulation parameters provide the leverage for achieving the desired angle of transmission for the two output beams of the STM beam splitter. In addition, unequal power division between the output beams can be achieved by varying the ST modulation parameters.

(4) Here, we present an application of obliquely illuminated STM slabs. Consequently, the scheme and results for the finite difference time-domain (FDTD) simulation results

*sajjad.taravati@utoronto.ca

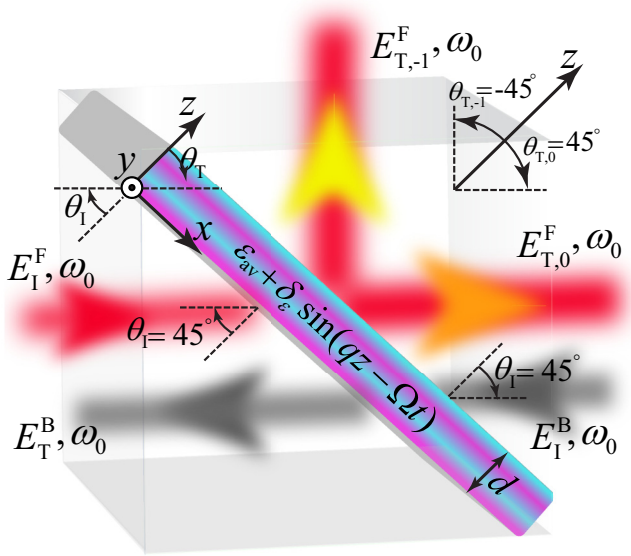

FIG. 1. Schematic of nonreciprocal beam splitting in a STM slab. The slab varies in time two times faster than the input wave.

for oblique incidence to a STM slab at microwave frequencies are presented.

(5) A closed-form solution is presented that provides a deep insight into the wave propagation inside the STM beam splitters and the difference between the subluminal, luminal, and superluminal ST modulations.

(6) The analysis of the STM beam splitter is further accomplished by investigation of its analytical three-dimensional dispersion diagrams, achieved by Bloch-Floquet decomposition of space-time harmonics (STHs).

Accordingly, the rest of the paper is structured as follows. Section II presents the operation principle of the proposed STM beam splitter. In Sec. III, we derive the analytical solution for oblique electromagnetic wave propagation inside the STM beam splitter based on the Bloch-Floquet representation of the electromagnetic fields. Then, Sec. IV presents the time and frequency domains numerical simulation results for the beam splitting and amplification in the STM beam splitter. Next, the closed form solution will be provided in Sec. V, which gives a leverage for understanding the wave propagation and transitions in STM structures. A short discussion on practical realization of superluminal STM structures at different frequencies will be presented in Sec. VI. Finally, Sec. VII concludes the paper.

II. OPERATION PRINCIPLE

Figure 1 sketches the nonreciprocal beam transmission and splitting in a STM slab. By appropriate design of the band structure, that is, the ST modulation format and its associated temporal and spatial modulation frequencies, unidirectional energy and momentum exchange between the incident wave-under angle of incidence and transmission $\theta_I = \theta_{T,0} = 45^\circ$ and temporal frequency ω_0 to the first lower STH-under angle of transmission $\theta_{T,-1} = -45^\circ$ and temporal frequency ω_0 will occur. Assuming TM_y or E_y polarization, the electric field of the incident light beam in the forward $+z$ direction may be expressed as

$$E^{F}_{I}(x,z,t) = E_0 e^{-i[k_x x + k_z z - \omega_0 t]}, \tag{1}$$

is traveling in the $+z$ direction under the angle of incidence $\theta_I = 45^\circ$, and impinges to the periodic STM slab. The x and z components of the spatial frequency read $k_x = k_0 \sin(\theta_I)$ and $k_z = k_0 \cos(\theta_I)$, respectively, in which $k_0 = \omega_0/v_b = \omega_0\sqrt{\epsilon_r}/c$, with ω_0 being the temporal frequency of the incident wave, v_b denoting the phase velocity in the background medium, ϵ_r representing the relative electric permittivity of the background medium, and c denoting the speed of light in vacuum. The STM slab assumes a sinusoidal ST-varying permittivity, as

$$\epsilon(z,t) = \epsilon_{av} + \delta_\epsilon \sin(qz - \Omega t), \tag{2}$$

where $\epsilon_{av} = \epsilon_r + \delta_\epsilon$ is the average permittivity of the slab, δ_ϵ denotes the modulation strength, $\Omega = 2\omega_0$ is the modulation temporal frequency, and

$$q = \frac{2k_0}{\gamma} \tag{3}$$

represents the spatial frequency of the modulation, with $\gamma = v_m/v_b$ being the ST velocity ratio, where v_m and v_b are the phase velocity of the modulation and the background medium, respectively. Since the slab permittivity is periodic in space and time, with spatial frequency q and temporal frequency $2\omega_0$, the electric field inside the slab may be decomposed into ST Bloch-Floquet waves as

$$\mathbf{E}_S(x,z,t) = \hat{\mathbf{y}} \sum_{m=-M}^{M} A_m e^{-i(k_x x + k_{z,m} z - \omega_m t)}, \tag{4a}$$

and

$$\begin{aligned}\mathbf{H}_S(x,z,t) &= \frac{1}{\eta_S}[\hat{\mathbf{k}}_S \times \mathbf{E}_S(x,z,t)] \\ &= \sum_{m=-M}^{M} \left[-\hat{\mathbf{x}}\frac{k_{z,m}}{\mu_0\omega_m} + \hat{\mathbf{z}}\frac{\sin(\theta_I)}{\eta_S}\right] \\ &\quad \times A_m e^{-i(k_x x + k_{z,m} z - \omega_m t)},\end{aligned} \tag{4b}$$

where $M \to \infty$ is the number of STHs. In Eq. (4), $\eta_S = \sqrt{\mu_0/(\epsilon_0\epsilon_r)}$, and A_m represents the unknown amplitude of the mth STH, characterized by the spatial frequency

$$k_{z,m} = \beta_0 + mq, \tag{4c}$$

and the temporal frequency

$$\omega_m = (1 + 2m)\omega_0, \tag{4d}$$

with β_0 being the unknown spatial frequency of the fundamental harmonic. The unknowns of the electric field, that is, A_m and β_0, will be found through satisfying Maxwell's equations.

The transmission angle of the mth transmitted STH, $\theta_{T,m}$, satisfies the Helmholtz relation as

$$k_0^2 \sin^2(\theta_I) + k_m^2 \cos^2(\theta_{T,m}) = k_m^2, \tag{5}$$

where $k_m = \omega_m/v_b$ denotes the wave number of the mth transmitted STH outside the STM slab. Solving Eq. (5) for

$\theta_{\mathrm{T},m}$ yields

$$\theta_{\mathrm{T},m} = \sin^{-1}\left(\frac{k_x}{k_m}\right) = \sin^{-1}\left(\frac{\sin(\theta_\mathrm{I})}{1+m\Omega/\omega_0}\right) = \sin^{-1}\left(\frac{\sin(\theta_\mathrm{I})}{1+2m}\right). \tag{6a}$$

Equation (6a) demonstrates the spectral decomposition of the transmitted wave. Consequently, the fundamental STH, $m = 0$, and the first lower STH, $m = -1$, with equal temporal frequency ω_0, will be, respectively, transmitted under the angles of transmission of

$$\theta_{\mathrm{T},0} = \theta_\mathrm{I} = 45^\circ, \quad \theta_{\mathrm{T},-1} = -\theta_\mathrm{I} = -45^\circ, \tag{6b}$$

so that they are transmitted under 90° angle difference, presenting the desired beam splitting. The scattering angle of the mth STH inside the STM slab reads

$$\theta_{\mathrm{S},m} = \tan^{-1}\left(\frac{k_x}{k_{z,m}}\right). \tag{7}$$

In addition, the transmitted electric fields from the slab are found as

$$\mathbf{E}_\mathrm{T}(x,z,t) = \mathbf{E}_\mathrm{S}(x,z,t)e^{-ik_{z,m}z} = \hat{\mathbf{y}}\sum_{m=-M}^{M} A_m e^{-i(k_x x + k_{z,m}[d+z]-\omega_m t)}. \tag{8}$$

The sourceless wave equation reads

$$\nabla^2\mathbf{E}_\mathrm{S}(x,z,t) - \frac{1}{c^2}\frac{\partial^2[\epsilon(z,t)\mathbf{E}_\mathrm{S}(x,z,t)]}{\partial t^2} = 0. \tag{9}$$

Substituting Eqs. (2) and (4) into Maxwell's equations yields a matrix equation as

$$[K]\vec{A} = 0, \tag{10a}$$

where $[K]$ is a $(2M+1)\times(2M+1)$ matrix with elements

$$K_{m,m} = \epsilon_\mathrm{av} - \frac{k_x^2 + k_{z,m}^2}{k_0^2}, \quad K_{m,m-1} = i\frac{\delta_\epsilon}{2}, \quad K_{m,m+1} = -i\frac{\delta_\epsilon}{2}, \tag{10b}$$

and where $\vec{A}$ represents a $(2M+1)\times 1$ vector containing A_m coefficients. Equation (10a) has a nontrivial solution if

$$\det\{[K]\} = 0. \tag{11}$$

Equation (11) represents the dispersion relation of the STM beam splitter which provides the unknown spatial frequency of the fundamental STH for a given frequency, i.e., $\beta_0(\omega_0)$. After finding the $\beta_0(\omega_0)$, the $[K]$ matrix in Eq. (10a) is known and therefore, the unknown amplitude of the STHs A_m will be calculated using Eq. (10a).

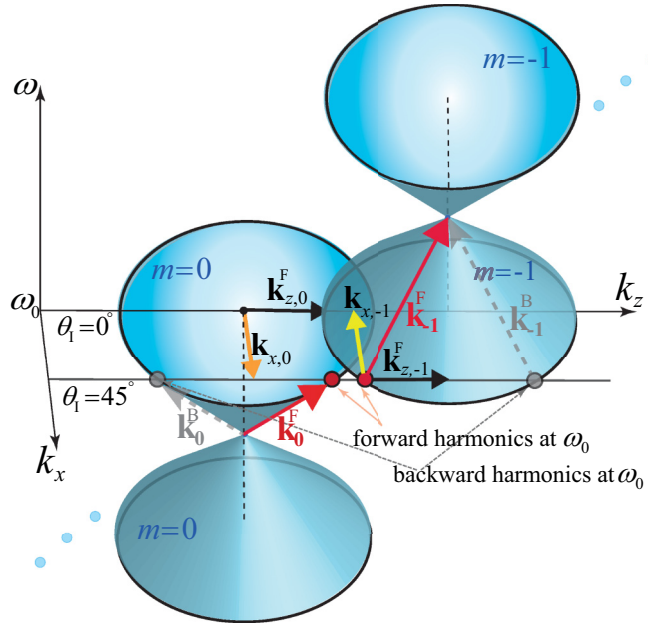

FIG. 2. Qualitative representation of the periodic three-dimensional dispersion diagram for the periodic STM slab in Fig. 1. The medium is under oblique illumination of $\theta_\mathrm{I} = 45^\circ$ at the fundamental harmonic $m = 0$, corresponding to the temporal frequency ω_0, where $\mathbf{k}_{x,0} = \hat{\mathbf{x}}k_x = \hat{\mathbf{x}}k_0\sin(\theta_\mathrm{I})$. The lower STH, $m = -1$, provides the same temporal frequency as the fundamental harmonic, $|\omega_m| = |\omega_0(1+2m)|_{m=-1} = \omega_0$, but opposite x component of the spatial frequency, that is, $\mathbf{k}_{x,-1} = -\hat{\mathbf{x}}k_x = -\hat{\mathbf{x}}k_0\sin(\theta_\mathrm{I})$.

III. ANALYTICAL 3D DISPERSION DIAGRAM

Figure 2 presents a qualitative illustration of the three-dimensional dispersion diagram in the STM medium in Fig. 1 achieved using Eq. (11). This diagram is formed by $2M+1$ periodic set of double cones (here, only $m = 0$ and $m = -1$ harmonics are shown), each of which represents a STH, with apexes at $k_x = 0$, $k_z = -mq$, and $\omega = -2m\omega_0$, and the slope of v_m with respect to the $k_z - k_x$ plane. Consider the oblique incidence of a wave, representing the fundamental harmonic $m = 0$ with temporal frequency ω_0, propagating along the $[+x, +z]$ direction. It is characterized by x and z components of the spatial frequency, $\mathbf{k}_x = \hat{\mathbf{x}}k_x$ and $\mathbf{k}_z^\mathrm{F} = \hat{\mathbf{z}}k_z$. The wave impinges to the medium under the angle of incidence $\theta_\mathrm{I} = 45^\circ$ and excites an infinite number of (we truncate it to $2M+1$) STH waves, with different spatial and temporal frequencies of $[k_x, k_{z,m}]$ and ω_m. However, interestingly, the first lower STH $m = -1$ offers similar characteristics as the fundamental harmonic, that is, the identical temporal frequency of ω_0 and identical z component of the spatial frequency of $\mathbf{k}_{z,-1}^\mathrm{F} = \mathbf{k}_{z,0}^\mathrm{F}$, but opposite x component of the spatial frequency of $\mathbf{k}_{x,-1} = -\mathbf{k}_{x,0}$. Hence, $m = -1$ harmonic propagates along the $[-x, +z]$ direction. In general the x component of the mth STH reads $\mathbf{k}_{x,m} = -\mathbf{k}_{x,-m-1}$. Moreover, since $\omega_m = \omega_{-m-1}$, the undesired STHs acquire temporal frequency of $2m\omega_0$ and far away from the fundamental harmonic. Thus, most of the incident energy is residing in $m = 0$ and $m = -1$ harmonics, both at ω_0, respectively, transmitted under $\theta_{\mathrm{T},0} = \theta_\mathrm{I}$ and $\theta_{\mathrm{T},-1} = -\theta_\mathrm{I}$ transmission angles with $2\theta_\mathrm{I}$ angle difference.

The exchange of the energy and momentum between the fundamental and first lower harmonic occurs only for the forward, $+z$, wave incidence. This is observed from Fig. 2, as the forward harmonics (red circles, where $\partial\omega/\partial k_z > 0$) are very close, whereas the backward harmonics (gray circles, where $\partial\omega/\partial k_z < 0$) are far apart from each other. Therefore, a nonreciprocal transition of energy is achieved from the incident wave under $\theta_{\rm I} = 45^\circ$ to the first STH under $\theta_{\rm T,-1} = -45^\circ$, through the ST modulation under $\theta_{\rm mod} = 0^\circ$.

Figure 3(a) shows the analytical solution for three-dimensional dispersion diagram of the STM medium in Fig. 1, computed using Eq. (11) for $\gamma = 1.2$. For a given frequency, this three-dimensional diagram provides the two-dimensional $k_z/q - k_x/q$ isofrequency diagram of the medium. Figure 3(b) plots the isofrequency diagram at $\omega/2\omega_0 = 0.5$ (or $\omega = \omega_0$), containing an infinite periodic set of circles centered at $(k_z/q, k_x/q) = (-m, 0)$ with radius $\gamma(0.5 + m)$.

It may be seen from Figs. 3(a) and 3(b) that at $\omega = \omega_0$, the $m = 0$ and $m = -1$ STHs offer identical isofrequency circles. However, their associated forward harmonics (red circles) are very close to each other whereas their associated backward harmonics (gray circles) are significantly separated. For a nonzero velocity ratio ($\gamma > 0$), the forward and backward STHs acquire different distances, i.e., $\Delta\beta^{\pm} = k^{\pm}_{z,m+1} - k^{\pm}_{z,m}$ [18]. Particularly, as γ increases, $\Delta\beta^-$ increases and $\Delta\beta^+$ decreases. As a result, at the limit of $\gamma = 1$ the forward harmonics acquire distances $\Delta\beta^+/q = 0$, and the backward harmonics acquire distances $\Delta\beta^-/q = 2$. Hence, increasing γ results in the significant enhancement in the nonreciprocity of the medium, so that the forward harmonic waves tend to merge together ($\Delta\beta^+ \to 0$) and exchange their energy and momentum, whereas the backward harmonics tend to separate from each other ($\Delta\beta^+ \to 2$) [Fig. 3(a)]. Hence, such a dynamic modulation has nearly no effect on the backward incident beam.

IV. NUMERICAL SIMULATION RESULTS

We next verify the above theory by FDTD numerical simulation of the dynamic process through solving Maxwell's equations. Figure 4 plots the implemented finite-difference time-domain scheme for numerical simulation of the oblique wave impinging to the STM beam splitter. We first discretize the medium to $K + 1$ spatial samples and $M + 1$ temporal samples, with the steps of Δz and Δt, respectively. Next, the finite-difference discretized form of the first two Maxwell's equations for the electric and magnetic fields [considering Eq. (4)] will be simplified to

$$H_x\big|^{i+1/2}_{j+1/2} = (1 - \Delta t) H_x\big|^{i-1/2}_{j+1/2} + \frac{\Delta t}{\mu_0 \Delta z}\left(E_y\big|^{i}_{j+1} - E_y\big|^{i}_{j}\right) \tag{12a}$$

$$H_z\big|^{i+1/2}_{j+1/2} = (1 - \Delta t) H_z\big|^{i-1/2}_{j+1/2} - \frac{\Delta t}{\mu_0 \Delta z}\left(E_y\big|^{i}_{j+1} - E_y\big|^{i}_{j}\right) \tag{12b}$$

$$E_y\big|^{i+1}_{j} = \left(1 - \frac{\Delta t \epsilon'\big|^{i}_{j}}{\epsilon\big|^{i+1/2}_{j}}\right) E_y\big|^{i}_{j} + \frac{\Delta t/\Delta z}{\epsilon\big|^{i+1/2}_{j}} \cdot \left[\left(H_x\big|^{i+1/2}_{j+1/2} - H_x\big|^{i+1/2}_{j-1/2}\right) - \left(H_z\big|^{i+1/2}_{j+1/2} - H_z\big|^{i+1/2}_{j-1/2}\right)\right], \tag{12c}$$

where $\epsilon' = \partial\epsilon(z,t)/\partial t = -\Omega\delta_\epsilon \cos(qz - \Omega t)$.

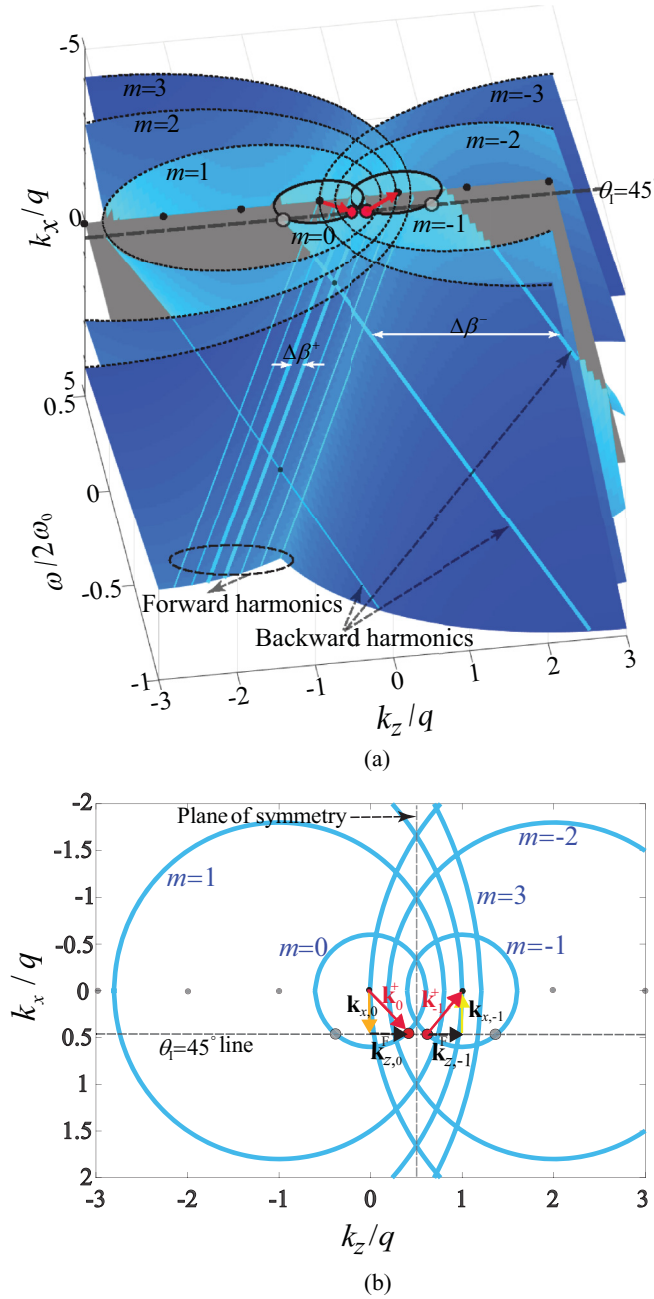

FIG. 3. Analytical dispersion diagram of the periodic STM slab in Fig. 1 for $\gamma = 1.2$ computed using Eq. (11). The forward incidence under $\theta_{\rm I} = 45^\circ$ corresponding to $k_x/q = 0.4243$ excites the $m = -1$ STH, resulting in a strong exchange of energy between $m = 0$ and $m = -1$ harmonics, with the identical temporal frequency of Ω_0. (a) Three-dimensional dispersion diagram constituted of an array of periodic cones [18]. (b) Isofrequency diagram at $\omega = \omega_0$ presents an infinite set of circles centered at $(k_z/q, k_x/q) = (-m, 0)$ with radius $\gamma(0.5 + m)$.

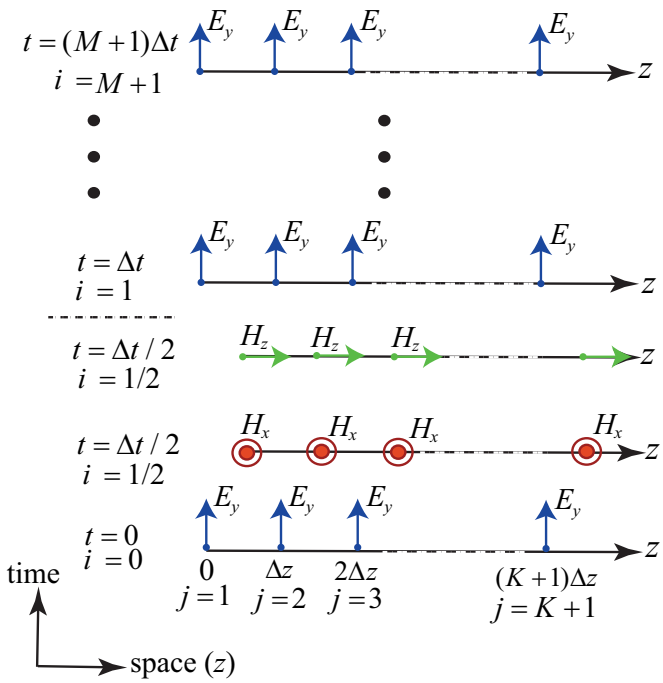

FIG. 4. General representation of the finite-difference time-domain scheme for numerical simulation of the oblique incidence of an E_y wave to STM beam splitter.

Figure 5 shows the numerical simulation results for the forward oblique wave incidence to the slab, shown in Fig. 1, with $\epsilon_r = 1$, $\delta_\epsilon = 0.2$, $\gamma = 1.2$, $d = 3\lambda_0 = 3 \times 2\pi/k_0$, $\theta_I = 45^\circ$, and $\omega_0 = 3$ GHz. It may be seen from this figure that an efficient beam splitting with significant transmission gain is achieved in the forward direction. Figures 6(a) and 6(b) provide the results for the oblique wave incidence from the right side and top, respectively, corresponding to $\theta_I = 45^\circ$ and $\theta_I = -45^\circ$. The presented analytical and numerical results demonstrate that the dynamic beam splitter provides a perfect

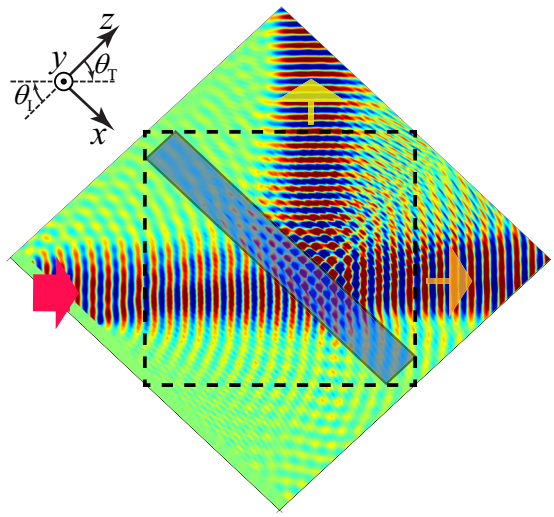

FIG. 5. Nonreciprocal beam splitting in periodically STM slab. FDTD numerical simulation for the forward wave incidence to the slab, from the left, with $\theta_I = 45^\circ$.

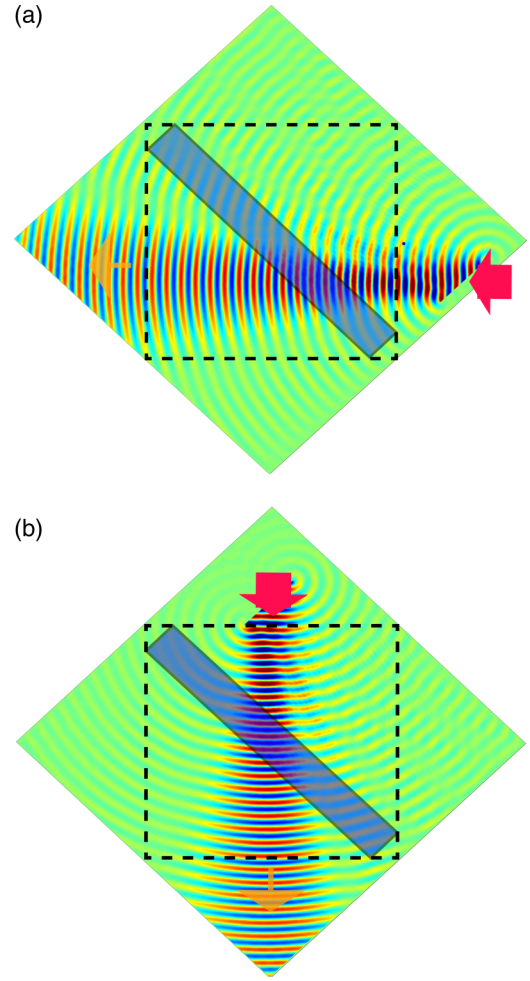

FIG. 6. Nonreciprocal beam splitting in periodically STM slab. FDTD numerical simulation for the wave incidence to the slab. (a) From the right with $\theta_I = 45^\circ$. (b) From the top, i.e., $\theta_I = -45^\circ$.

nonreciprocal beam splitting, in the lack of beam tilting. In contrast to conventional passive beam splitters, here the beam splitting is achieved for a noncollimated beam. It may be shown that by changing the modulation parameters, i.e., γ, θ_I and ϵ_{av}, tunable transmission angles, unequal splitting ratio, and unequal angles of transmission will be achieved. Figure 7 compares the analytical and numerical results for the spectrum of the incident and transmitted electric fields in Fig. 5. This figure shows that 3dB transmission gain is achieved for each of the transmitted beams in the forward excitation. Figure 7 demonstrates that the undesired higher order harmonics, at $\omega = 2m\omega_0$, are sufficiently weak so that the beam splitter safely operates at single frequency ω_0.

V. CLOSED FORM SOLUTION FOR ELECTROMAGNETIC FIELDS

It is shown in Sec. IV that by proper design of the band structure, a pure unidirectional beam splitting can be achieved in a obliquely illuminated STM slab. The analytical solution of the electromagnetic fields based on the double Bloch-Floquet decomposition of electromagnetic fields, presented in Sec. III, provides an accurate solution for the fields

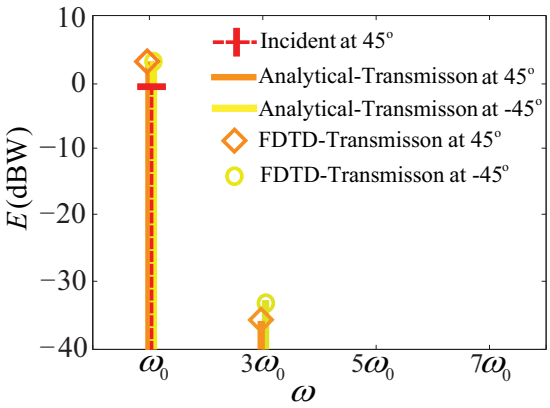

FIG. 7. Comparison of the analytical and numerical results for the frequency spectrum of the incident and transmitted electric fields in Fig. 5, i.e., wave incidence to the slab from the left with $\theta_{\rm I} = 45^{\circ}$.

scattered by such a slab, which is very useful. However, such an analytical solution does not provide a deep insight into the wave propagation inside the slab. In particular, it is of great interest to have an intuitive explanation about the effect of different parameters, e.g., δ_ϵ, γ, k_x, and k_z, on the wave propagation and energy exchange between the incident field $m = 0$ and the excited first lower harmonic $m = -1$. Moreover, the accurate analytical solution, based on the mathematical modeling presented in Sec. III, is achieved through a substantial computational cost. To resolve this issue, here we provide an approximate closed form solution for the electromagnetic fields propagating inside and transmitted from the STM beam splitter, which provides a clear picture of the transition between the incident and the first lower STHs.

As we showed in the previous section, given the weak transition of energy and momentum from the fundamental STH $m = 0$ to higher order STHS except $m = -1$, the electric field inside the STM slab can be represented based on the superposition of the aforementioned two STHs, i.e., $m = 0$ and $m = -1$. The electric field is then defined by

$$E_{\rm S}(x,z,t) = a_0(z)e^{-i(k_x x + k_z z - \omega_0 t)} + a_{-1}(z)e^{i(-k_x x + (q-k_z)z - \omega_0 t)}, \tag{13}$$

where $a_0(z)$ and $a_{-1}(z)$ are the unknown field coefficients. We shall stress that here the field coefficients are z dependent since they include both the amplitude and the change in the spatial frequency (wave number) introduced by the ST modulation. Following the procedure provided in the Supplemental Material in Ref. [43], we insert the electric fields in (13) into the wave equations in (9) and achieve a coupled differential equation for the field coefficients, i.e.,

$$\frac{d}{dz}\begin{bmatrix} a_0(z) \\ a_{-1}(z) \end{bmatrix} = \begin{bmatrix} M_0 & C_0 \\ C_{-1} & M_{-1} \end{bmatrix}\begin{bmatrix} a_0(z) \\ a_{-1}(z) \end{bmatrix}, \tag{14a}$$

where

$$M_0 = \frac{ik_0^2}{2k_z}(\epsilon_{\rm av} - \epsilon_{\rm r}),$$

$$M_{-1} = \frac{ik_0^2}{2(k_z - q)}\left[\epsilon_{\rm av} - \epsilon_{\rm r}\frac{k_x^2 + (q-k_z)^2}{k_0^2}\right],$$

$$C_0 = i\frac{\delta k_0^2}{4k_z},$$

$$C_{-1} = i\frac{\delta k_0^2}{4(k_z - q)}. \tag{14b}$$

The solution to the coupled differential equation in (14a) is given by [43]

$$a_0(z) = \frac{E_0}{2\Delta}\left((M_0 - M_{-1} + \Delta)e^{\frac{M_0+M_{-1}+\Delta}{2}z} - (M_0 - M_{-1} - \Delta)e^{\frac{M_0+M_{-1}-\Delta}{2}z}\right), \tag{15a}$$

$$a_{-1}(z) = \frac{E_0 C_{-1}}{\Delta}\left(e^{\frac{M_0+M_{-1}+\Delta}{2}z} - e^{\frac{M_0+M_{-1}-\Delta}{2}z}\right), \tag{15b}$$

where $\Delta = \sqrt{(M_0 - M_{-1})^2 + 4C_0C_{-1}}$. For a given ST modulation ratio γ, the field coefficients in Eq. (15) acquire different forms. In general, ST modulation is classified into three categories, i.e., subluminal ($0 < \gamma < 1$ or $v_{\rm m} < v_{\rm b}$), luminal ($\gamma \to 1$ or $v_{\rm m} \to v_{\rm b}$), and superluminal ($\gamma > 1$ or $v_{\rm m} > v_{\rm b}$).

A. Subluminal and superluminal ST modulations

Considering $\epsilon_{\rm av} = \epsilon_{\rm r}$, the $a_0(z)$ and $a_{-1}(z)$ in Eq. (15) would be a periodic sinusoidal function with respect to z, if $\Delta = \sqrt{(M_0 - M_{-1})^2 + 4C_0C_{-1}}$ is imaginary, i.e., $(M_0 - M_{-1})^2 + 4C_0C_{-1} < 0$. By solving this, we achieve an interval for the luminal ST modulation, that is,

$$\gamma_{\rm sub} < \frac{1}{\sqrt{\epsilon_{\rm av} + \delta_\epsilon}} \leqslant \gamma_{\rm lum} \leqslant \frac{1}{\sqrt{\epsilon_{\rm av} - \delta_\epsilon}} < \gamma_{\rm sup}, \tag{16}$$

where $\gamma_{\rm sub}$, $\gamma_{\rm lum}$, and $\gamma_{\rm sup}$ are the ST velocity ratio for subluminal, luminal, and superluminal ST modulations, respectively. The interval for luminal ST modulation is called sonic regime in analogy with sonic boom effect in acoustics, where an airplane travels with the same speed or faster than the speed of sound. It should be noted that the luminal ST modulation interval in Eq. (16) is exactly the same as the one achieved from the exact analytical solution [17,18,25].

Figure 8(a) plots the closed form and FDTD numerical simulation results for the absolute electric field coefficient inside the slab, with the wave incidence from the left side (forward incidence), considering superluminal ST modulation of $\gamma = 1.2$ and $\delta_\epsilon = 0.28$. It is seen from this figure that both $a_0(z)$ and $a_{-1}(z)$ possess periodic sinusoidal form and exhibit a substantial transmission gain at $z = 3\lambda_0$. Such a transmission gain is tuned through the variation of γ and δ_ϵ. This result is consistent with the transmission gain achieved in the FDTD numerical simulation results in Figs. 5 and 7. The coherence length $l_{\rm c}$, where both $a_0(z)$ and $a_{-1}(z)$ acquire their maximum amplitude is found as [43]

$$l_{\rm c} = \pi\left(\left[\frac{k_0^2[\epsilon_{\rm av} - \epsilon_{\rm r}]/k_z - q}{(\gamma-2)/(\gamma-1)}\right]^2 + \frac{\delta^2 k_0^4}{4k_z(k_z - q)}\right)^{-1}. \tag{17}$$

Figure 8(b) plots the result for the superluminal STM slab in Fig. 8(a), except for wave incidence from the right side

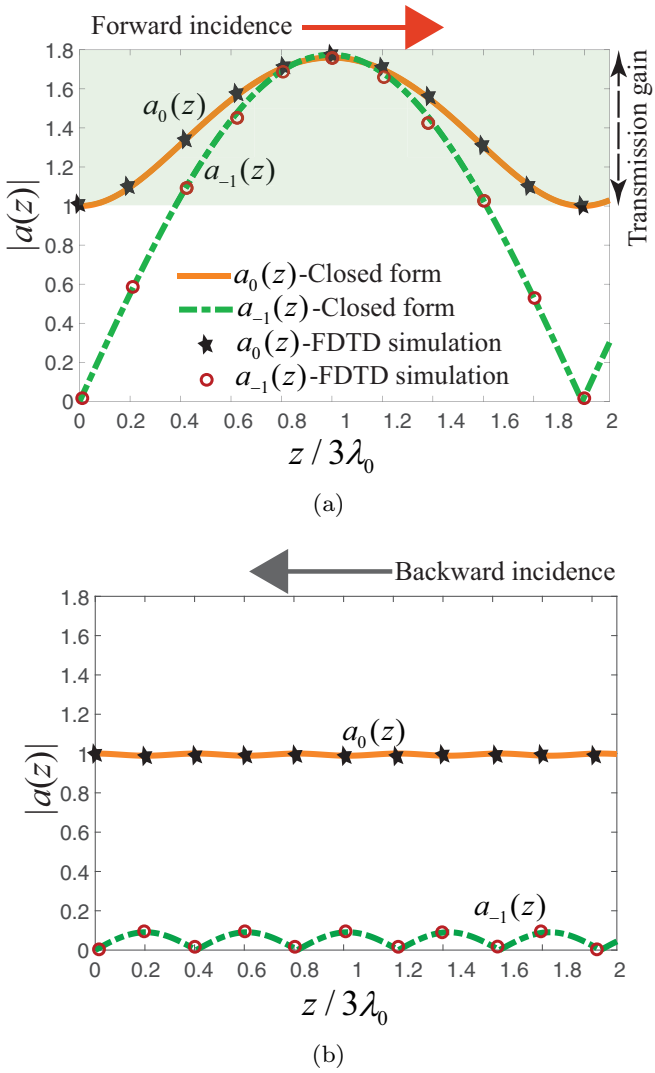

FIG. 8. Closed-form solution results and the FDTD numerical simulation results for the z-dependent absolute field coefficients in Eq. (13), i.e., $a_0(z)$ and $a_{-1}(z)$, inside the superluminal STM beam splitter, with $\gamma = 1.2$ and $\delta_\epsilon = 0.28$. (a) Forward wave incidence, where the wave propagates from left to right. (b) Backward wave incidence, where the wave propagates from right to left.

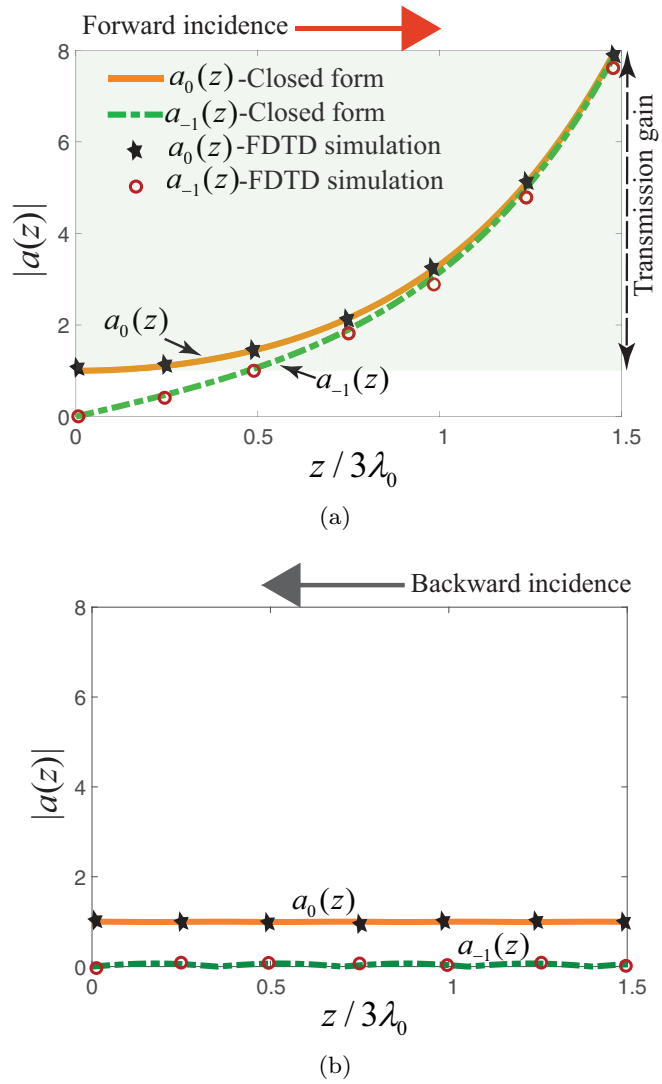

FIG. 9. Closed-form solution results and the FDTD numerical simulation results for the z-dependent absolute field coefficients in Eq. (13), i.e., $a_0(z)$ and $a_{-1}(z)$, inside the luminal STM beam splitter, with $\gamma = 1$ and $\delta_\epsilon = 0.28$. (a) Forward wave incidence, where the wave propagates from left to right. (b) Backward wave incidence, where the wave propagates from right to left.

(backward incidence). It may be seen from this figure that, in contrast to the forward wave incidence where a substantial exchange of the energy and momentum between the $m = 0$ and $m = -1$ STHs are achieved, here the incident wave passes through the slab with negligible alteration and minor transition of energy and momentum to the $m = -1$ STH. This is obviously in agreement with the nonreciprocal response presented in Figs. 5, 6(a), and 6(b).

B. Luminal ST modulation

It may be shown that for the luminal ST modulation, where $\gamma \to 1$, the field coefficients in Eq. (15), $a_0(z)$ and $a_{-1}(z)$, acquire pure real (or complex) forms. This yields exponential growth of the electric field amplitude along the STM slab. Hence, considering $\gamma = 1$, the total electric field inside the STM slab reads

$$E_S(x,z,t)|_{\gamma=1} = E_0 \cosh\left(\frac{\delta k_0^2}{4k_z} z\right) e^{-i(k_x x + k_z z - \omega_0 t)} - i\frac{\delta k_0^2}{2k_z} E_0 \sinh\left(\frac{\delta k_0^2}{4k_z} z\right) e^{i(-k_x x + (q-k_z) z - \omega_0 t)}. \tag{18}$$

Figure 9(a) plots the closed form and FDTD numerical simulation results for the absolute value of the electric field coefficients $a_0(z)$ and $a_{-1}(z)$ inside the luminal ($\gamma = 1$ and $\delta_\epsilon = 0.28$) STM slab for forward wave incidence. It may be seen from this figure that both $a_0(z)$ and $a_{-1}(z)$ possess a nonperiodic exponentially growing profile and exhibit a substantial transmission gain at $z \geqslant 3\lambda_0$. It should be noted that the solutions for the field coefficients presented in Eqs. (15) and (18) are very useful and provide a deep insight into

the wave propagation inside the STM slab, especially for the luminal ST modulation (sonic regime), where the Bloch-Floquet-based analytical solution does not exist since the solution does not converge [17,18,25].

Figure 9(b) plots the result for the luminal STM slab in Fig. 9(a), except for wave incidence from the right side (backward incidence). This figure shows that, in contrast to the forward wave incidence, here the incident wave passes through the slab with negligible alteration and minor transition of energy and momentum to the $m = -1$ STH.

VI. DISCUSSION ON PRACTICAL REALIZATION OF SUPERLUMINAL ST MODULATION

To practically realize superluminal ST modulation (here $\gamma = 1.2$), the phase velocity of the modulation should be greater than the velocity of the incident wave in the background (unmodulated) medium and not the velocity of light in vacuum [15]. Considering a glass as the background medium with permittivity >1.5, achieving $\gamma = 1.2$ would be realistic. For instance, one may use coupled structures with two different lines (possessing different phase velocities) for the input wave and the modulation [30,42,44]. In such structures a modulation velocity greater than at least one of the characteristic velocities involved is required. In general, the way of achieving the fast pumping depends on the frequency range, as follows.

(i) At low frequencies, one may use filter constants which are appropriately selected for two weakly coupled transmission lines [18,30,42,44], one for the pump and one for the main incident wave.

(ii) At ultrahigh frequencies, a serpentine transmission line supports the propagation of the main incident wave [45], which lowers the phase velocity relative to the modulation velocity.

(iii) At microwave frequencies the pump wave is supported in a closed waveguide [46], thereby achieving a fast phase velocity.

In addition, recently, there has been an experimental demonstration of time-modulated structure [47], where the medium is periodically modulated in time only, representing the limiting case of an infinite modulation velocity, i.e., $q = 0$ and hence $v_m = \Omega/q \to \infty$.

VII. CONCLUSION

We have introduced a unidirectional beam splitter and amplifier based on asymmetric coherent photonic transitions in obliquely illuminated space-time-modulated (STM) media. The operation of this dynamic beam splitter is demonstrated by both the analytical, closed-form, and numerical simulation results. While the normally illuminated STM media have been previously used for the realization of various components, including insulators, parametric amplifiers, and nonreciprocal frequency generators, this paper presents a study investigating the oblique illumination of STM media. Accordingly, this paper proposed a forward-looking application of such dynamic media. The proposed unidirectional beam splitter is endowed with unique functionalities, including adjustable one-way transmission gain, tunable splitting angle and arbitrary unequal splitting power ratio, as well as high isolation, and hence, is expected to substantially reduce the source and isolation requirements of communication systems.

[1] C. M. F. Schneider, On-chip superconducting microwave beam splitter, Master's thesis, Technische Universität München, 2014.

[2] J. Hammer, S. Thomas, P. Weber, and P. Hommelhoff, Microwave Chip-Based Beam Splitter for Low-Energy Guided Electrons, Phys. Rev. Lett. **114**, 254801 (2015).

[3] B.-K. Tan and G. Yassin, A planar beam splitter for millimeter and submillimeter heterodyne mixer array, IEEE Trans. Terahertz Sci. Technol. **7**, 664 (2017).

[4] R. Watanabe, A novel polarization-independent beam splitter, IEEE Trans. Microw. Theory Techn. **28**, 685 (1980).

[5] W. Zhu, J. Shaker, J. S. Wight, M Cuhaci, and D. A. McNamara, Microwave spatial beam splitter/combiner using artificial microwave volume hologram technology, Electron. Lett. **42**, 1 (2006).

[6] R.-B. Hwang, N.-C. Hsu, and C.-Y. Chin, A spatial beam splitter consisting of a near-zero refractive index medium, IEEE Trans. Antennas Propagat. **60**, 417 (2012).

[7] J. R. Cooper, S. Kim, and M. M. Tentzeris, A novel polarization-independent, free-space, microwave beam splitter utilizing an inkjet-printed, 2-D array frequency selective surface, IEEE Antennas Wirel. Propagat. Lett. **11**, 686 (2012).

[8] A. Wallraff, D. I. Schuster, A. Blais, L. Frunzio, R.-S. Huang, J. Majer, S. Kumar, S. M. Girvin, and R. J. Schoelkopf, Strong coupling of a single photon to a superconducting qubit using circuit quantum electrodynamics, Nature (London) **431**, 162 (2004).

[9] A. Blais, R.-S. Huang, A. Wallraff, S. M. Girvin, and R. J. Schoelkopf, Cavity quantum electrodynamics for superconducting electrical circuits: An architecture for quantum computation, Phys. Rev. A **69**, 062320 (2004).

[10] M. Mariantoni, F. Deppe, A. Marx, R. Gross, F. K. Wilhelm, and E. Solano, Two-resonator circuit quantum electrodynamics: A superconducting quantum switch, Phys. Rev. B **78**, 104508 (2008).

[11] A. A. Houck, D. I. Schuster, J. M. Gambetta, J. A. Schreier, B. R. Johnson, J. M. Chow, L. Frunzio, J. Majer, M. H. Devoret, S. M. Girvin, and R. J. Schoelkopf, Generating single microwave photons in a circuit, Nature (London) **449**, 328 (2007).

[12] D. Bozyigit, C. Lang, L. Steffen, J. M. Fink, C. Eichler, M. Baur, R. Bianchetti, P. J. Leek, S. Filipp, A. Wallraff, M. P. Da Silva, and A. Blais, Correlation measurements of individual microwave photons emitted from a symmetric cavity, J. Phys.: Conf. Ser. **264**, 012024 (2011).

[13] D. Bozyigit, C. Lang, L. Steffen, J. M. Fink, C. Eichler, M. Baur, R. Bianchetti, P. J. Leek, S. Filipp, M. P. Da Silva, and A. Blais, Antibunching of microwave-frequency photons observed in correlation measurements using linear detectors, Nat. Phys. **7**, 154 (2011).

[14] M. Mariantoni, E. P. Menzel, F. Deppe, M. A. A. Caballero, A. Baust, T. Niemczyk, E. Hoffmann, E. Solano, A. Marx, and R. Gross, Planck Spectroscopy and Quantum Noise of Microwave Beam Splitters, Phys. Rev. Lett. **105**, 133601 (2010).

[15] E. S. Cassedy, Dispersion relations in time-space periodic media: Part II-unstable interactions, Proc. IEEE **55**, 1154 (1967).

[16] Z. Yu and S. Fan, Complete optical isolation created by indirect interband photonic transitions, Nat. Photonics **3**, 91 (2009).

[17] S. Taravati, Giant Linear Nonreciprocity, Zero Reflection, and Zero Band Gap in Equilibrated Space-Time-Varying Media, Phys. Rev. Appl. **9**, 064012 (2018).

[18] S. Taravati, N. Chamanara, and C. Caloz, Nonreciprocal electromagnetic scattering from a periodically space-time modulated slab and application to a quasisonic isolator, Phys. Rev. B **96**, 165144 (2017).

[19] M. M. Salary, S. Jafar-Zanjani, and H. Mosallaei, Time-varying metamaterials based on graphene-wrapped microwires: Modeling and potential applications, Phys. Rev. B **97**, 115421 (2018).

[20] M. M. Salary, S. Jafar-Zanjani, and H. Mosallaei, Electrically tunable harmonics in time-modulated metasurfaces for wavefront engineering, New J. Phys. **20**, 123023 (2018).

[21] S. Taravati and A. A. Kishk, Advanced wave engineering via obliquely illuminated space-time-modulated slab, IEEE Trans. Antennas Propagat. **67**, 270 (2019).

[22] A. L. Cullen, A traveling-wave parametric amplifier, Nature (London) **181**, 332 (1958).

[23] P. K. Tien, Parametric amplification and frequency mixing in propagating circuits, J. Appl. Phys. **29**, 1347 (1958).

[24] P. K. Tien and H. Suhl, A traveling-wave ferromagnetic amplifier, Proc. IRE **46**, 700 (1958).

[25] E. S. Cassedy and A. A. Oliner, Dispersion relations in time-space periodic media: Part I-stable interactions, Proc. IEEE **51**, 1342 (1963).

[26] J. L. Wentz, A nonreciprocal electrooptic device, Proc. IEEE **54**, 97 (1966).

[27] S. Bhandare, S. K. Ibrahim, D. Sandel, H. Zhang, F Wust, and R. Noé, Novel nonmagnetic 30-dB traveling-wave single-sideband optical isolator integrated in III/V material, IEEE J. Sel. Top. Quantum Electron. **11**, 417 (2005).

[28] H. Lira, Z. Yu, S. Fan, and M. Lipson, Electrically Driven Nonreciprocity Induced by Interband Photonic Transition on a Silicon Chip, Phys. Rev. Lett. **109**, 033901 (2012).

[29] N. Chamanara, S. Taravati, Z. Deck-Léger, and C. Caloz, Optical isolation based on space-time engineered asymmetric photonic bandgaps, Phys. Rev. B **96**, 155409 (2017).

[30] S. Taravati, Self-biased broadband magnet-free linear isolator based on one-way space-time coherency, Phys. Rev. B **96**, 235150 (2017).

[31] JunHwan Kim, S. Kim, and G. Bahl, Complete linear optical isolation at the microscale with ultralow loss, Sci. Rep. **7**, 1647 (2017).

[32] D. B. Sohn, S. Kim, and G. Bahl, Time-reversal symmetry breaking with acoustic pumping of nanophotonic circuits, Nat. Photon. **12**, 91 (2018).

[33] Y. Hadad, D. L. Sounas, and A. Alù, Space-time gradient metasurfaces, Phys. Rev. B **92**, 100304 (2015).

[34] Y. Shi and S. Fan, Dynamic non-reciprocal meta-surfaces with arbitrary phase reconfigurability based on photonic transition in meta-atoms, Appl. Phys. Lett. **108**, 021110 (2016).

[35] Yu. Shi, S. Han, and S. Fan, Optical circulation and isolation based on indirect photonic transitions of guided resonance modes, ACS Photonics **4**, 1639 (2017).

[36] Z. Wu and A. Grbic, A transparent, time-modulated metasurface, in *2018 12th International Congress on Artificial Materials for Novel Wave Phenomena (Metamaterials)* (IEEE, Espoo, Finland, 2018), pp. 439–441.

[37] S. Taravati, Aperiodic space-time modulation for pure frequency mixing, Phys. Rev. B **97**, 115131 (2018).

[38] S. Qin, Q. Xu, and Yuanxun Ethan Wang, Nonreciprocal components with distributedly modulated capacitors, IEEE Trans. Microw. Theory Techn. **62**, 2260 (2014).

[39] N. A. Estep, D. L. Sounas, J. Soric, and A. Alù, Magnetic-free non-reciprocity and isolation based on parametrically modulated coupled-resonator loops, Nat. Phys. **10**, 923 (2014).

[40] N. Reiskarimian, A. Nagulu, T. Dinc, and H. Krishnaswamy, Integrated conductivity-modulation-based rf magnetic-free nonreciprocal components: Recent results and benchmarking, IEEE Antennas Wirel. Propagat. Lett. **17**, 1978 (2018).

[41] S. Taravati and C. Caloz, Space-time modulated nonreciprocal mixing, amplifying and scanning leaky-wave antenna system, in *IEEE AP-S Int. Antennas Propagat. (APS)* (Vancouver, Canada, 2015).

[42] S. Taravati and C. Caloz, Mixer-duplexer-antenna leaky-wave system based on periodic space-time modulation, IEEE Trans. Antennas Propagat. **65**, 442 (2017).

[43] See Supplemental Material at http://link.aps.org/supplemental/10.1103/PhysRevB.99.075101 for detailed derivations.

[44] S. Okwit and E. W. Sard, Constant-output-frequency, octave tuning range backward-wave parametric amplifier, IRE Transactions on Electron Devices **8**, 540 (1961).

[45] S. Okwit, M. I. Grace, and E. W. Sard, UHF backward-wave parametric amplifier, IRE Transactions on Microwave Theory and Techniques **10**, 558 (1962).

[46] H. Hsu, Backward traveling-wave parametric amplifiers, in *Solid-State Circuits Conference, Digest of Technical Papers, 1960 IEEE International*, Vol. 3 (IEEE, Philadelphia, PA, USA, 1960), pp. 91–92.

[47] J. Reyes-Ayona and P. Halevi, Electromagnetic wave propagation in an externally modulated low-pass transmission line, IEEE Trans. Microwave Theory Tech. **64**, 3449 (2016).